

## Article

# Quantitative Analysis of Water Injection Mass and Timing Effects on Oxy-Fuel Combustion Characteristics in a GDI Engine Fuelled with E10

Hao Chen <sup>1</sup>, Chenxi Wang <sup>2,\*</sup>, Xiang Li <sup>3,\*</sup> , Yongzhi Li <sup>4</sup>, Miao Zhang <sup>5</sup>, Zhijun Peng <sup>6</sup>, Yiqiang Pei <sup>2</sup>, Zhihao Ma <sup>1</sup>, Xuewen Zhang <sup>3</sup>, Peiyong Ni <sup>3</sup>, Rohitha Weerasinghe <sup>7</sup> and Raouf Mobasher <sup>8,9</sup> 

<sup>1</sup> School of Vehicle and Traffic Engineering, Henan University of Science and Technology, Luoyang 471023, China

<sup>2</sup> State Key Laboratory of Engines, Tianjin University, Tianjin 300072, China

<sup>3</sup> School of Mechanical Engineering, Nantong University, Nantong 226019, China

<sup>4</sup> Y&C Engine Co., Ltd., Wuhu 241080, China

<sup>5</sup> Yijiahe Technology Co., Ltd., Shenzhen 518028, China

<sup>6</sup> School of Engineering, University of Lincoln, Lincoln LN6 7TS, UK

<sup>7</sup> School of Computer Science and Technology, University of Bedfordshire, Luton LU1 3JU, UK

<sup>8</sup> UMR 9189-CRISTAL-Centre de Recherche en Informatique Signal et Automatique de Lille, CNRS, University Lille, F-59000 Lille, France

<sup>9</sup> Junia, Smart Systems and Energies, F-59000 Lille, France

\* Correspondence: wangcx1342@tju.edu.cn (C.W.); xiang.li@ntu.edu.cn (X.L.)

**Abstract:** The climate change issue has become a growing concern due to the increasing greenhouse gas emissions. To achieve carbon neutrality for mitigating the climate problem, the oxy-fuel combustion (OFC) technique on internal combustion engines (ICEs) has attracted much attention. Furthermore, the water injection (WI) strategy was proven effective in improving the combustion process and thermal efficiency in engines under OFC mode. However, WI strategy effects on gasoline direct injection (GDI) engines fuelled with gasoline–alcohol blends have not been reported. This study quantitatively analysed WI mass and timing effects on oxy-fuel combustion performance from a GDI engine fuelled with E10 (10% ethanol and 90% gasoline in mass) by simulation. The results show that equivalent brake-specific fuel consumption (BSFC<sub>E</sub>) shows a monotonically decreasing trend with the increase in the water–fuel mass ratio ( $R_{wf}$ ) from 0 to 0.2. However, further increasing  $R_{wf}$  would cause a deterioration in BSFC<sub>E</sub> due to the enhanced cooling effects of water vaporisation. Moreover, an appropriate water injection timing ( $t_{WI}$ ) could be explored for improving OFC performance, especially for large  $R_{wf}$  conditions. The difference in BSFC<sub>E</sub> between  $t_{WI} = -100^\circ\text{CA}$  and  $t_{WI} = -60^\circ\text{CA}$  can be up to around 6.3 g/kWh by increasing  $R_{wf}$  to 0.6.

**Keywords:** oxy-fuel combustion (OFC); water injection (WI); gasoline direct injection (GDI) engine; E10; simulation



**Citation:** Chen, H.; Wang, C.; Li, X.; Li, Y.; Zhang, M.; Peng, Z.; Pei, Y.; Ma, Z.; Zhang, X.; Ni, P.; et al. Quantitative Analysis of Water Injection Mass and Timing Effects on Oxy-Fuel Combustion Characteristics in a GDI Engine Fuelled with E10. *Sustainability* **2023**, *15*, 10290. <https://doi.org/10.3390/su151310290>

Academic Editor: Francesco Nocera

Received: 11 May 2023

Revised: 27 June 2023

Accepted: 27 June 2023

Published: 29 June 2023



**Copyright:** © 2023 by the authors. Licensee MDPI, Basel, Switzerland. This article is an open access article distributed under the terms and conditions of the Creative Commons Attribution (CC BY) license (<https://creativecommons.org/licenses/by/4.0/>).

## 1. Introduction

In the past few years, global warming concerns have become more serious, and extreme heat conditions appear more frequently [1]. Achieving the goals of carbon peaking and carbon neutrality has been proposed to minimise carbon dioxide (CO<sub>2</sub>) emissions for mitigating global warming issues. Hence, various carbon reduction technologies have been implemented in the transportation sector, such as battery electric vehicles (BEVs) [2], ammonia or hydrogen fuel engines [3,4], and fuel cell vehicles [5]. These technologies have attracted much attention because of their carbon-free characteristics. However, it is still very valuable and attractive to achieve CO<sub>2</sub> capture and storage for internal combustion engines (ICEs), which account for the largest proportion of transportation power sources nowadays.

As shown in the chemical process of Equation (1), the combustion products of oxy-fuel combustion (OFC) technology proposed by Yaverbaum are almost  $\text{CO}_2$  and  $\text{H}_2\text{O}$ , which has been an attractive alternative for decreasing and capturing carbon emissions [6–9]. Figure 1 shows a schematic diagram of a novel OFC system with carbon capture and storage (CCS) in the application of ICE. During the working process, intake air can be replaced by pure oxygen and  $\text{CO}_2$  from exhaust gas recirculation (EGR). Hence, without  $\text{N}_2$  involved in combustion,  $\text{NO}_x$  emissions can be totally eliminated. Moreover, the extra  $\text{CO}_2$  can be compressed by a compressor after separating from  $\text{H}_2\text{O}$ , and then easily captured and stored into a tank.

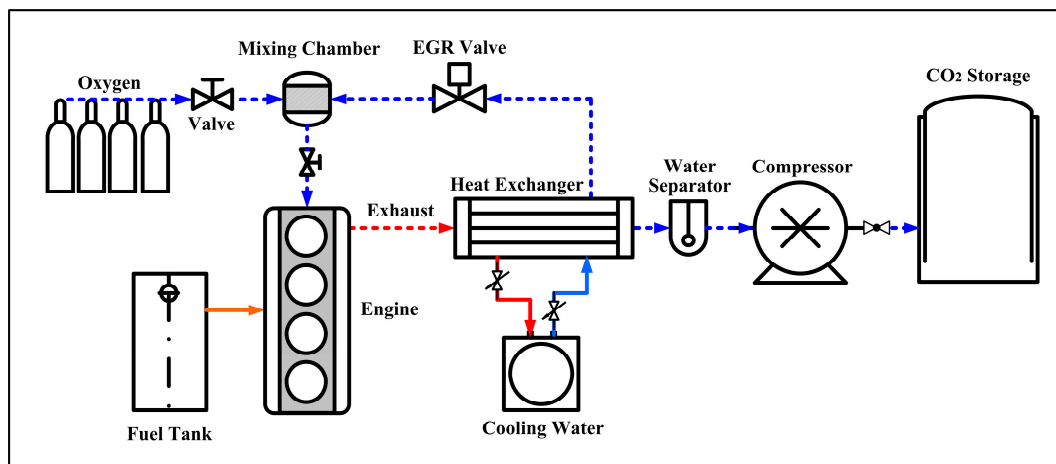


**Figure 1.** Configuration of OFC technology in ICE.

When comparing OFC mode to conventional air combustion (CAC) mode, the differences in physicochemical properties between  $\text{CO}_2$  and  $\text{N}_2$  should be noticed and stressed, as shown in Table 1 [10,11]. First and foremost, the molecular weight of  $\text{CO}_2$  is 57% higher than that of  $\text{N}_2$ . Moreover, the specific heat capacity of  $\text{CO}_2$  is 106% of  $\text{N}_2$ . Hence, compared to  $\text{N}_2$ , the mole heat capacity of  $\text{CO}_2$  is considerably higher, which would negatively impact the combustion rates and temperature under OFC mode. Second, the thermal diffusivity of  $\text{CO}_2$  is only 64.4% of  $\text{N}_2$ . Moreover, the mass diffusivity speed of  $\text{O}_2$  in  $\text{CO}_2$  is 22.2% lower than the conditions of  $\text{N}_2$ . These factors can help reduce the heat release rate and slow chemical reactions during the early combustion stage. Moreover, the thermal conductivity of  $\text{CO}_2$  is very close to that of  $\text{N}_2$ , which would not easily cause discrepancies in the combustion.

Hence, although using OFC technology in engines has excellent potential for carbon reduction, controlling the engine combustion process and maintaining thermal efficiency under OFC mode is challenging. Ditaranto et al. [12] indicated that the low thermal diffusivity properties of  $\text{CO}_2$  would lead to more heat loss than conventional air combustion, resulting in lower thermal efficiency. It was also found that the flame characteristics in OFC mode are closely related to the oxygen concentration. Li et al. [13] conducted some numerical investigations of OFC combustion on dual-fuel spark ignition (SI) engines. The results suggested that with the increase in oxygen mass fraction, significant changes can be seen in combustion characteristics, leading to a reduction in brake-specific fuel consumption (BSFC). Yu et al. [14] reported that a high oxygen fraction could accelerate combustion and improve the maximum pressure rise rate. It indicated that pure  $\text{O}_2$  with no inert gas would produce an excessively fast combustion rate accompanying abnormal pressure rise rates of more than 4 MPa/CA. The powerful waves of engine super knock would rapidly occur across the combustion chamber with substantial amplitude, significantly damaging the engine.

**Table 1.** Physicochemical properties of CO<sub>2</sub> and N<sub>2</sub> (1000 k, 0.1 MPa) [10,11].

Property	CO <sub>2</sub>	N <sub>2</sub>	Ratio (CO <sub>2</sub> /N <sub>2</sub> )
Molecular weight	44	28	157%
Specific heat capacity (kJ/kgK)	1.2343	1.1674	106%
Kinematic viscosity (m <sup>2</sup> /s)	$7.69 \times 10^{-5}$	$1.2 \times 10^{-4}$	63.1%
Thermal diffusivity (m <sup>2</sup> /s)	$1.1 \times 10^{-4}$	$1.7 \times 10^{-4}$	64.4%
Mass diffusivity of O <sub>2</sub> (m <sup>2</sup> /s)	$9.8 \times 10^{-5}$	$1.3 \times 10^{-4}$	77.8%
Thermal conductivity (W/mK)	$7.057 \times 10^{-2}$	$6.599 \times 10^{-2}$	107%
Prandtl number	0.7455	0.7022	106%
Emissivity and absorptivity	>0	~0	-

Moreover, in order to further improve the combustion process and thermal efficiency, the water injection (WI) strategy has been implemented for engines under OFC mode. Bilger et al. [15] proposed a new conception of the internal combustion Rankine cycle (ICRC) engine, which employs preheated water directly injected into engine cylinders to control combustion. The key research progresses on the effects of WI strategy on the combustion characteristics in engines under OFC mode over the past decade are summarised in Table 2.

**Table 2.** Research summary of WI strategy in engines under OFC mode.

Publication Year	Focusing Parameter	Engine Type	Fuel	Main Authors
2013	WI mass, timing, pressure	PFI, SI	Propane	Yu et al. [14]
2014	WI temperature	PFI, SI	Propane	Fu et al. [16]
2014	WI mass, temperature	PFI, SI	Propane	Wu et al. [17]
2017	WI mass	HCCI, CI	N-heptane	Kang et al. [18]
2018	WI mass, timing, temperature	CI	N-heptane	Kang et al. [19]
2021	WI mass, timing, temperature	Dual-injection, SI	Gasoline	Li et al. [20]

Based on a single-cylinder port fuel injection (PFI) engine fuelled with propane, Yu et al. [14] studied the combustion performance under a quasi-ICRC engine after replacing air with oxygen as an oxidant. The study demonstrated that adding water to the combustion chamber could inhibit the spontaneous combustion of the air–fuel mixture by reducing the in-cylinder temperature. Meanwhile, the engine thermal efficiency could be improved by extending the constant pressure process caused by water evaporation at the beginning of the power stroke. Fu et al. [16] demonstrated that owing to the acceleration of the water vaporisation process, a higher WI temperature would help further improve cylinder pressure and engine thermal efficiency in a PFI engine under ICRC mode. For example, under the conditions of 2.9 ms fuel injection duration and 120 °C WI temperature, the engine indicated work and indicated thermal efficiency could be improved by 10.3% and 3.1%, respectively. Wu et al. [17] provided new insights into the solution for improving thermal efficiency by investigating the effects of WI duration and pressure in a PFI engine under OFC mode. It was reported that the thermal efficiency could be improved from 32.1% to 41.5%, and the higher WI pressure can make greater use of vaporisation heat, leading to higher thermal efficiency. Kang et al. [18] designed a WI system to explore its potential in stabilising the combustion process in an N-heptane homogeneous charge compression ignition (HCCI) engine under OFC mode. It was found that a suitable WI strategy helps maintain the engine thermal efficiency and mitigate combustion instability. A strategy using 120 °C and 35 MPa WI would be helpful to eliminate the phenomenon of abnormal combustion. Based on KIVA, Kang et al. [19] established a CFD model of an oxy-fuel diesel engine fuelled with N-heptane to study the feasibility of utilising WI strategies in affecting engine thermal efficiency. The study demonstrated that combustion stability is sensitive to WI timing, which can be fixed near the engine top dead centre of firing. In addition, Li et al. [20] investigated WI effects on OFC characteristics in a dual-injection SI engine fuelled

with gasoline. The research indicated that all three fuel injection conditions of GDI, 50% PFI plus 50% GDI and PFI would lead to different performances of cylinder pressure and combustion phasing by changing the value of WI mass, timing, or temperature. It demonstrated that appropriate WI strategies would be beneficial in optimising key combustion characteristics, which leads to relatively low fuel consumption.

From existing studies of OFC engines, the WI strategy has been proven as a potential benefit for the combustion process and thermal efficiency. Most of these studies focused on engines fuelled with propane, N-heptane, or gasoline. However, almost no research was reported about the effects of WI strategies on a gasoline direct injection (GDI) engine fuelled with gasoline–alcohol blends. Furthermore, with more stringent emission regulations in recent years, ethanol has been a clean burning fuel and common additive worldwide with the advantages of reducing emissions and enhancing anti-knock capacity.

Therefore, a quantitative analysis was provided in this study for investigating the WI mass and timing effects on OFC characteristics in a GDI engine fuelled with E10 (10% ethanol and 90% gasoline in mass, which is 9.3% ethanol and 90.7% gasoline in volume). The impacts of WI on OFC GDI engines fuelled with the gasoline–ethanol blend were initially explored. The findings of this study will significantly contribute to understanding the role of WI in the OFC process. Furthermore, the findings will provide novel information and theoretical guidance for improving the fuel economy of GDI engines fuelled with E10 under OFC mode.

## 2. Research Approach and Numerical Method

### 2.1. Engine and Experimental Facilities

The engine test was conducted on a 2.0-litre turbocharged four-cylinder GDI engine. The details of the engine technical specifications are listed in Table 3, and the schematic diagram of the engine testbed is presented in Figure 2.

**Table 3.** Engine specifications.

Item	Content
Engine type	Four-cylinder; four-stroke
Bore × Stroke (mm)	82.5 × 92
Displacement (L)	2.0
Fuel system	GDI
Intake system	Turbocharged
Compression ratio	9.6:1
Rated speed (rpm)	5500
Rated power (kW)	160
Maximum torque (N·m)	320

During the test, an electrical dyno and a programable electronic control unit (ECU) were mainly used to control the key engine operating parameters, such as speed, torque, ignition, and fuel injection timing. The transient cylinder pressure traces were measured with plug-type transducers (AVL-GH13Z), an amplifier (Kistler 5018A), and a combustion analyser (AVL 641).

To eliminate the cycle-to-cycle fluctuations' interference, the average cylinder pressure from two hundred consecutive cycles was used in this work. The spark timings were optimised to be the minimum advance for maximum brake torque (MBT) or the knock-limited spark advance (KLSA). Before the test, E10 fuel was obtained by thoroughly mixing 10% ethanol with 90% gasoline in mass (9.3% ethanol and 90.7% gasoline in volume). The properties of the gasoline and ethanol are listed in Table 4.

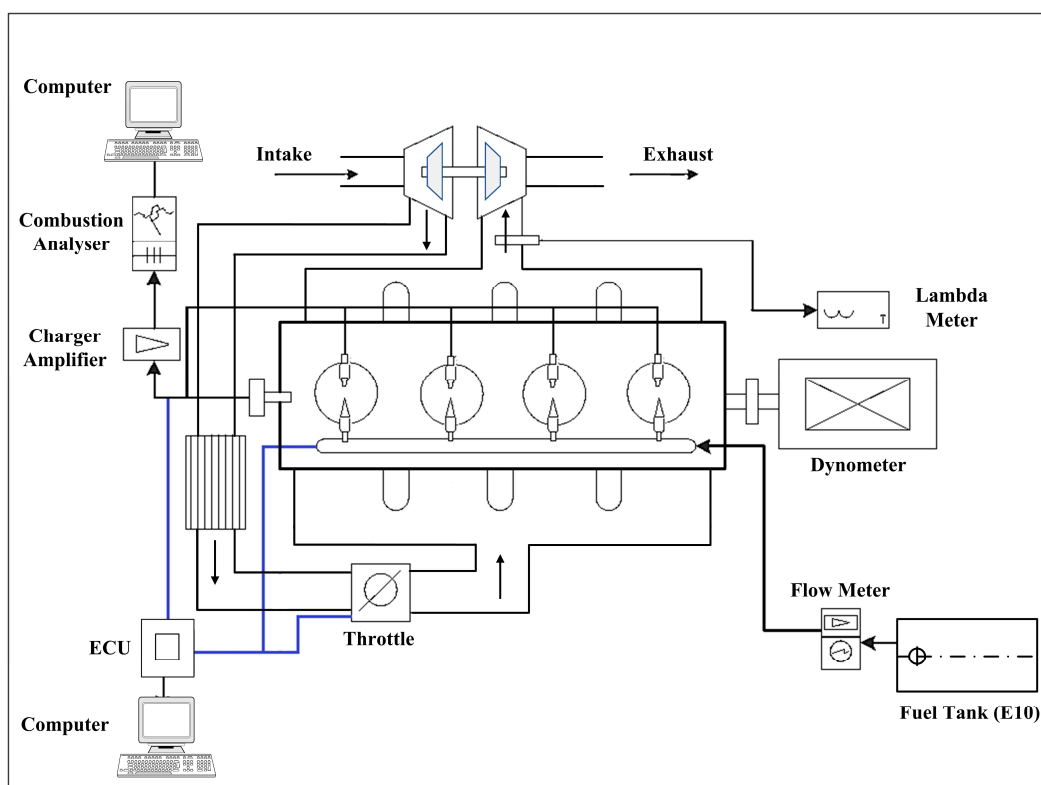


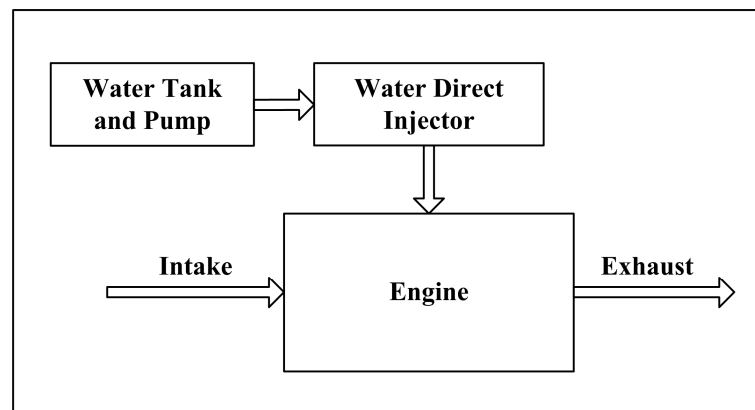
Figure 2. Schematic diagram of engine testbed.

Table 4. Fuel properties [13].

Fuel Type	Ethanol	Gasoline
Chemical formula	$C_2H_5OH$	C5-C12
Density (20 °C) (kg/L)	0.789	0.73
Relative molecular mass	46	95–120
Gravimetric oxygen content (%)	34.78	<1
Research octane number	107	95
Boiling range (°C)	78	30–200
Kinematic viscosity (20 °C) ( $mm^2/s$ )	1.52	0.71
Dynamic viscosity (20 °C) (mPa·s)	1.2	0.52
Low heating value (kJ/kg)	26,900	44,300
Surface tension (20 °C) (mN/m)	21.97	22
Latent heat of vaporisation (kJ/kg)	840	370
Laminar flame speed (20 °C) (m/s)	0.5	0.33
Stoichiometric air–fuel ratio	8.95	14.7

## 2.2. Research Approach and Model Description

In this study, an engine model was established and developed by GT-Power, which has been widely used in the research of SI engines [21,22]. The settings of pipe geometry, engine displacement, cylinder, valve profile, and other parameters were consistent with engine specifications. The engine of this study was operated at 2000 rpm–10 bar brake mean effective pressure (BMEP), a typical medium-high load of engine urban operating conditions. The conversion from CAC mode to OFC mode in this simulation is achieved by replacing  $N_2$  with  $CO_2$ . Figure 3 presents the design of the WI components adopted in this study, which can directly inject water into the cylinder and are more convenient for practical engine implementation.



**Figure 3.** Schematic diagram of WI strategy.

Throughout this study, the WI pressure and water temperature are kept at 60 bar and 298 K, respectively. As shown in Equation (2), WI mass is represented by the water/fuel ratio ( $R_{wf}$ ) to make the parameters more visual. In addition, the other key parameters are fixed to control the variables in the investigation process, such as the intake oxygen mass fraction, intake temperature, and throttle angle.

$$R_{wf} = \frac{m_{water}}{m_{fuel}} \quad (2)$$

where  $m_{water}$  and  $m_{fuel}$  are water and fuel injection mass per engine working cycle, respectively.

$t_{WI}$  represents the WI timing.  $\varphi_{CA50}$  is the crank angle (CA) at 50% of cumulative released heat;  $P_M$  is the peak value of cylinder pressure. The equivalent brake-specific fuel consumption ( $BSFC_E$ ) is used to assess the fuel consumption, as shown in Equation (3) [23]. Compared to BSFC, the advantage of  $BSFC_E$  is that different fuels can be converted to equivalent gasoline consumption based on heating values [24–27].

$$BSFC_E = \frac{\tau_F \times 1000}{P} \times \frac{(0.1 \times H_E) \times (0.9 \times H_G)}{H_G} \quad (3)$$

where  $P$  (kW) is engine brake power;  $\tau_F$  (kg/h) is the fuel consumption rate of oxygen and fuel under actual conditions; and  $H_E$  and  $H_G$  are the low heating value of ethanol and gasoline, respectively.

In order to accurately predict the combustion process and heat transfer processes, “SI turbulent flame combustion” and “Woschni” submodels are chosen in this study, as shown in Equations (4) and (5) [28].

$$S_L = \left( B_m - B_\varnothing (\varnothing - \varnothing_m)^2 \right) \left( \frac{T_u}{T_{ref}} \right)^\alpha \left( \frac{p}{p_{ref}} \right)^\beta f(D) \quad (4)$$

where  $S_L$  is laminar flame speed;  $B_m$  is maximum laminar speed;  $B_\varnothing$  is laminar speed roll-off value;  $\varnothing$  is in-cylinder equivalence ratio;  $\varnothing_m$  is equivalence ratio at maximum speed;  $T_u$  is unburned gas temperature;  $T_{ref}$  is 298 K;  $p$  is pressure;  $p_{ref}$  is 101.325 kPa;  $\alpha$  is temperature exponent;  $\beta$  is pressure exponent; and  $f(D)$  is the dilution effect.

$$h = 110d^{-0.2}P^{0.8}T^{-0.53} \left[ C_1c_m + C_2 \frac{V_S T_1}{P_1 V_1} (P - P_0) \right]^{0.8} \quad (5)$$

where  $h$  is the heat transfer coefficient;  $d$  is the cylinder bore diameter;  $P$  is the cylinder pressure;  $T$  is the in-cylinder mean gas temperature;  $C_1$  is a constant related to the airflow velocity coefficient;  $c_m$  is the mean piston speed;  $C_2$  is a constant related to the

combustion chamber;  $V_5$  is the cylinder volume;  $T_1$ ,  $P_1$ , and  $V_1$  are cylinder temperature, pressure, and volume, respectively; and  $P_0$  is the cylinder pressure at the beginning of the compression stroke.

### 3. Results and Discussion

#### 3.1. Model Validation

In order to ensure the accuracy of the simulation results, it was necessary to perform model validation. Moreover, the model's effectiveness was further guaranteed and enhanced by checking the time-step sensitivity. Figure 4 presents the comparison of the cylinder pressure between the experimental and simulation results in the conditions of 2000 rpm-2 bar, 2000 rpm-6 bar, and 2000 rpm-10 bar under CAC mode. The corresponding torques of these conditions are 31.8 N·m, 95.4 N·m, and 159 N·m, respectively. It can be found that the curves' peaks of simulation are just around 2% higher than those of the experiment. Moreover, the peaks' locations of the relevant curves are well matched. In general, the overall trends of cylinder pressure match well, indicating that the model is capable of making a reliable prediction.

#### 3.2. Quantitative Analysis of WI Mass on OFC Performance

In this section, the first step is to optimise the engine spark timing to be MBT under OFC mode without WI. The relevant trends for BSFC<sub>E</sub> and  $\varphi_{CA50}$  can be seen in Figure 5.

With the spark timing advances from  $-58^\circ\text{CA}$  to  $-72^\circ\text{CA}$ , BSFC<sub>E</sub> decreases from 321.078 g/kWh to 311.35 g/kWh, which is the lowest value of the presented curve. Meanwhile,  $\varphi_{CA50}$  has an apparent change of  $8.6^\circ\text{CA}$ , which advances from  $11.8^\circ\text{CA}$  to  $3.2^\circ\text{CA}$ . However, with further advancing spark timing from  $-72^\circ\text{CA}$  to  $-90^\circ\text{CA}$ , BSFC<sub>E</sub> shows an obvious growing trend and reaches 320.827 g/kWh at  $-90^\circ\text{CA}$  spark timing.  $\varphi_{CA50}$  shows a monotonous decrease tendency from  $3.2^\circ\text{CA}$  to  $-6.2^\circ\text{CA}$ . The deterioration of BSFC<sub>E</sub> is closely related to the excessive early  $\varphi_{CA50}$ , which would negatively impact the effective use of energy, leading to a deterioration in BSFC<sub>E</sub>. Hence, it is found that  $-72^\circ\text{CA}$  is the optimal spark timing, which was fixed as a base in this study.

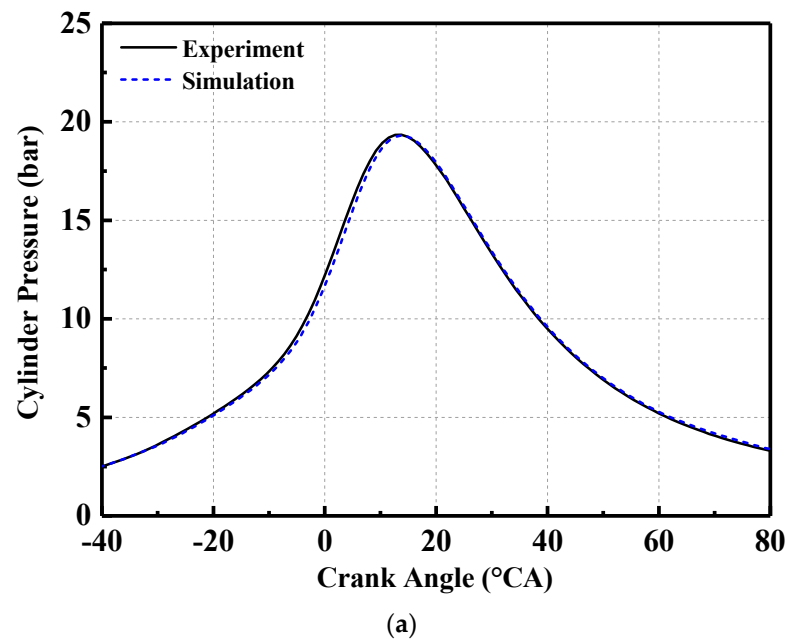
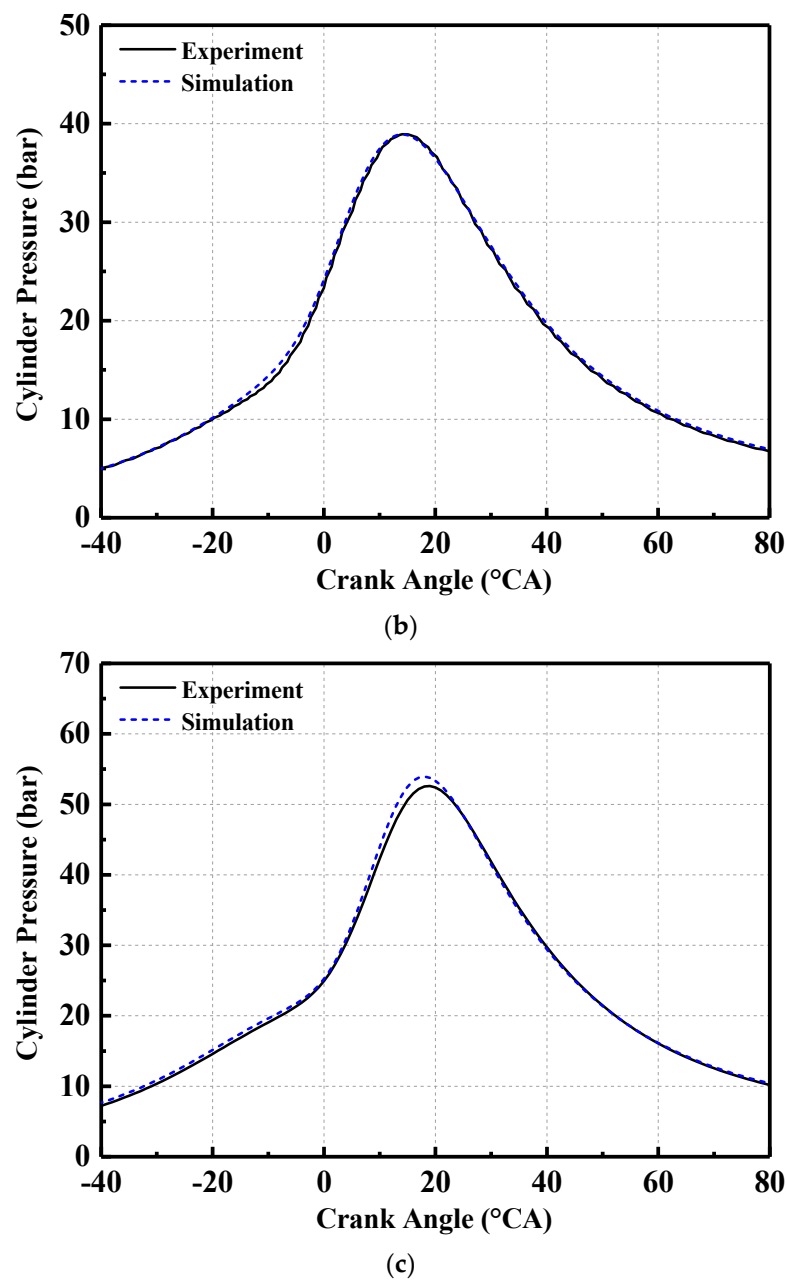


Figure 4. Cont.



**Figure 4.** Comparison of cylinder pressure in the conditions of 2000 rpm-2 bar, 2000 rpm-6 bar, and 2000 rpm-10 bar. (a) 2000 rpm-2 bar, (b) 2000 rpm-6 bar, (c) 2000 rpm-10 bar.

In order to explore the effects of WI mass on OFC performance, this section mainly evaluates  $BSFC_E$ , in-cylinder temperature, heat-release rate (HRR),  $P_M$  and  $\varphi_{CA50}$  under different  $R_{wf}$ . In addition, to focus on the quantitative analysis of WI mass,  $t_{WI}$  is fixed at  $-60^\circ CA$  in the study of this section.

As shown in Figure 6,  $R_{wf}$  has a significant influence on  $BSFC_E$ . Compared to other conditions, a relatively low level of  $BSFC_E$  can be found under the condition of zero water injection ( $R_{wf} = 0$ ). By increasing  $R_{wf}$  from 0 to 0.2,  $BSFC_E$  shows a monotonically decreasing trend and reaches a minimum of 310.836 g/kWh at  $R_{wf} = 0.2$ . This phenomenon can be attributed to the increase in oxygen concentration caused by injecting water [14]. When  $R_{wf}$  is larger than 0.2, a rebound trend occurs. By further increasing  $R_{wf}$ ,  $BSFC_E$  rises rapidly and achieves a maximum of 323.445 g/kWh at  $R_{wf} = 0.9$ . Afterwards,  $BSFC$  stabilises at approximately 323 g/kWh, indicating that the deterioration is counteracted

by increased oxygen concentration. The variation of  $R_{wf}$  can be further explained and explored through the results of the combustion characteristics, as follows.

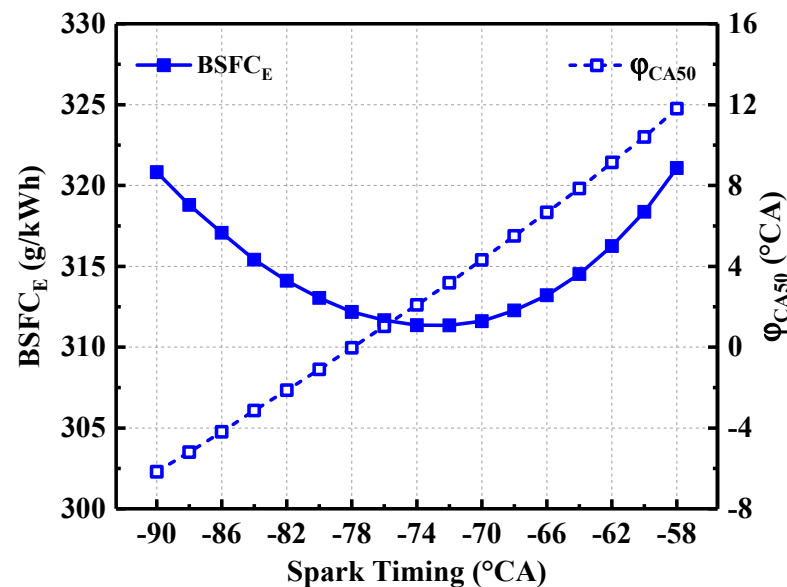


Figure 5. BSFC<sub>E</sub> and  $\varphi_{CA50}$  with varying spark timings.

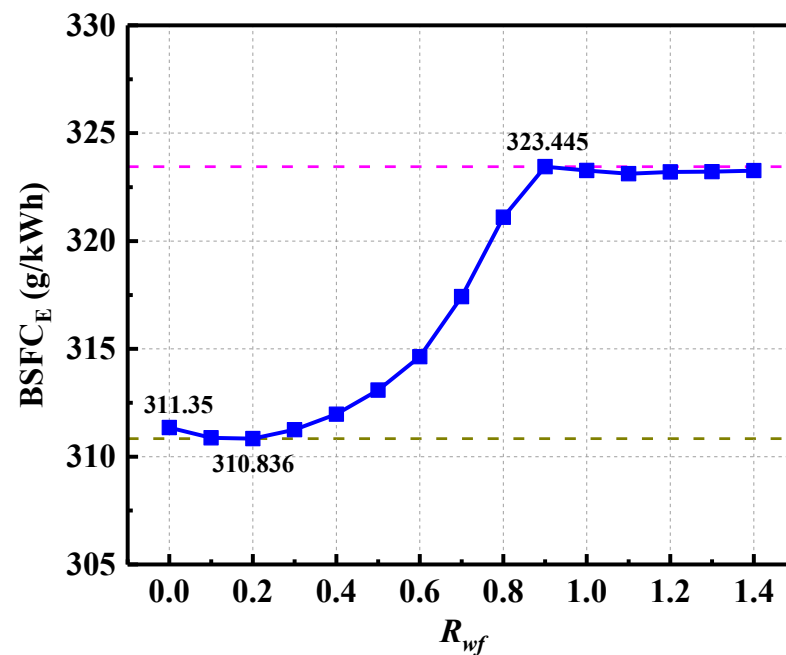


Figure 6. Effects of  $R_{wf}$  on BSFC<sub>E</sub>.

Figure 7 shows the effects of  $R_{wf}$  on the in-cylinder temperature. The shapes and locations of these in-cylinder temperature curves are generally similar. However, a downward trend can be found by increasing  $R_{wf}$ . The maximum in-cylinder temperature decreases from 2227 K to 2108 K with the increase in  $R_{wf}$  from 0 to 0.3. Subsequently, the maximum values reduce to 2001 K, 1950 K, and 1941 K under the conditions of  $R_{wf} = 0.6$ ,  $R_{wf} = 0.9$ , and  $R_{wf} = 1.2$ , respectively. This trend is mainly attributed to the enhanced effects of heat absorption with a large amount of vapourised water, which could effectively decrease the in-cylinder temperature.

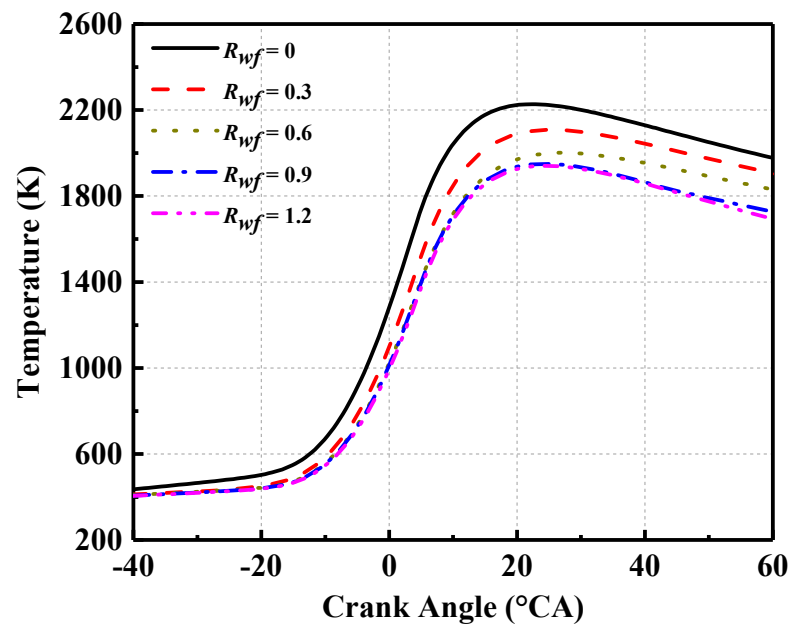


Figure 7. Effects of  $R_{wf}$  on in-cylinder temperature.

With the increase in  $R_{wf}$ , HRR shows a similar tendency with that of the in-cylinder temperature, as presented in Figure 8. Under the conditions of  $R_{wf} = 0$  or  $R_{wf} = 0.3$ , the peaks of the HRR curves are higher than for other conditions. The variations of in-cylinder temperature and HRR suggest that WI could obviously inhibit the heat release process of a GDI engine fuelled with E10 under OFC mode.

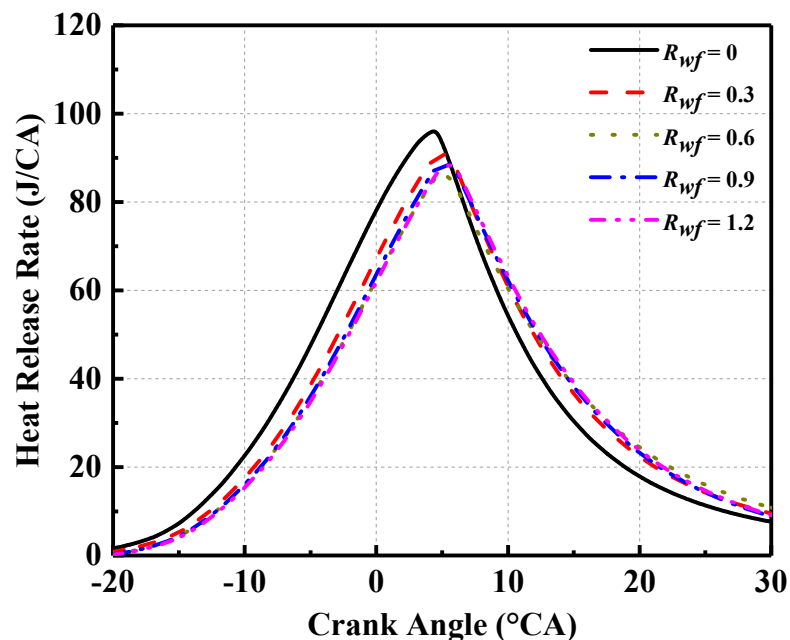


Figure 8. Effects of  $R_{wf}$  on HRR.

Regarding the  $P_M$  and  $\varphi_{CA50}$ , it can be seen that by increasing  $R_{wf}$  from 0 to 0.6,  $P_M$  has a gradual reduction from 54.6 bar to 49.8 bar and  $\varphi_{CA50}$  is postponed from  $3.2^\circ\text{CA}$  to  $5.7^\circ\text{CA}$ , as shown in Figure 9. Moreover, when  $R_{wf}$  is larger than 0.6,  $P_M$  and  $\varphi_{CA50}$  are generally stable. This demonstrates that although a large amount of injected water could provide more working medium and a higher oxygen concentration, the combustion

phasing is still retarded because of the strong cooling effects during water vaporisation, leading to an adverse impact on BSFC<sub>E</sub>.

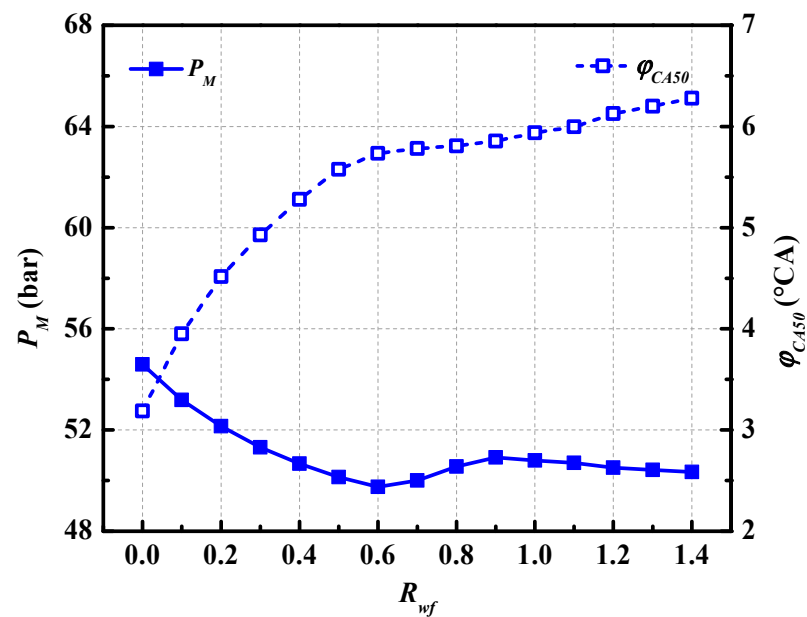


Figure 9. Effects of  $R_{wf}$  on  $P_{max}$  and  $\phi_{CA50}$ .

### 3.3. Quantitative Analysis of WI Timing on OFC Performance

As a key influencing factor, the effects of  $t_{WI}$  on OFC performance should also be clearly noted. Figure 10 shows the impacts of  $t_{WI}$  on BSFC<sub>E</sub>. In general, under the conditions of small  $R_{wf}$ , BSFC<sub>E</sub> remains at a relatively stable level by changing  $t_{WI}$ . In particular, BSFC<sub>E</sub> is largely unaffected by  $t_{WI}$  when  $R_{wf}$  is 0.1 and 0.2. The lowest value of BSFC<sub>E</sub> is 310.735 g/kWh, which appears at  $t_{WI} = -100^\circ\text{CA}$  and  $R_{wf} = 0.1$ .

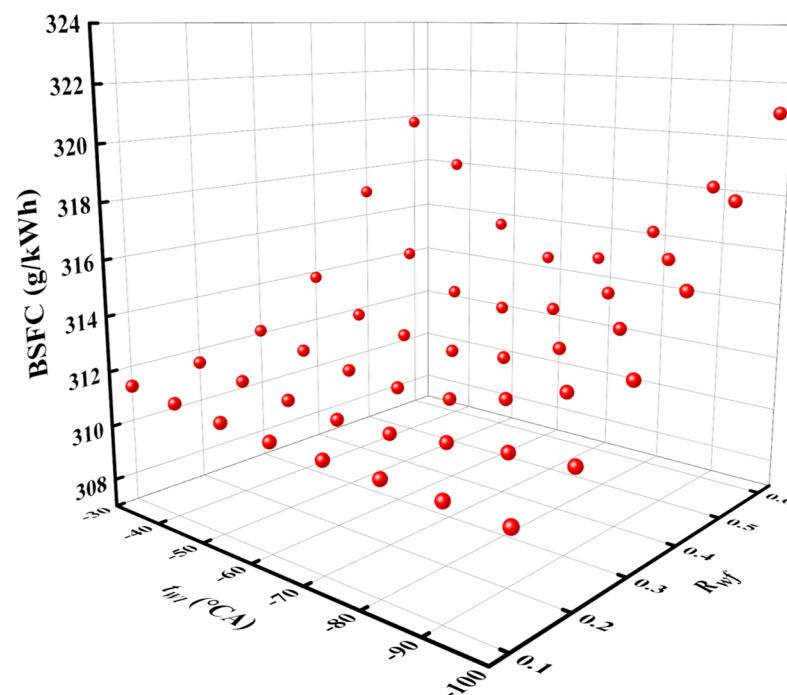


Figure 10. Effects of  $t_{WI}$  on BSFC<sub>E</sub>.

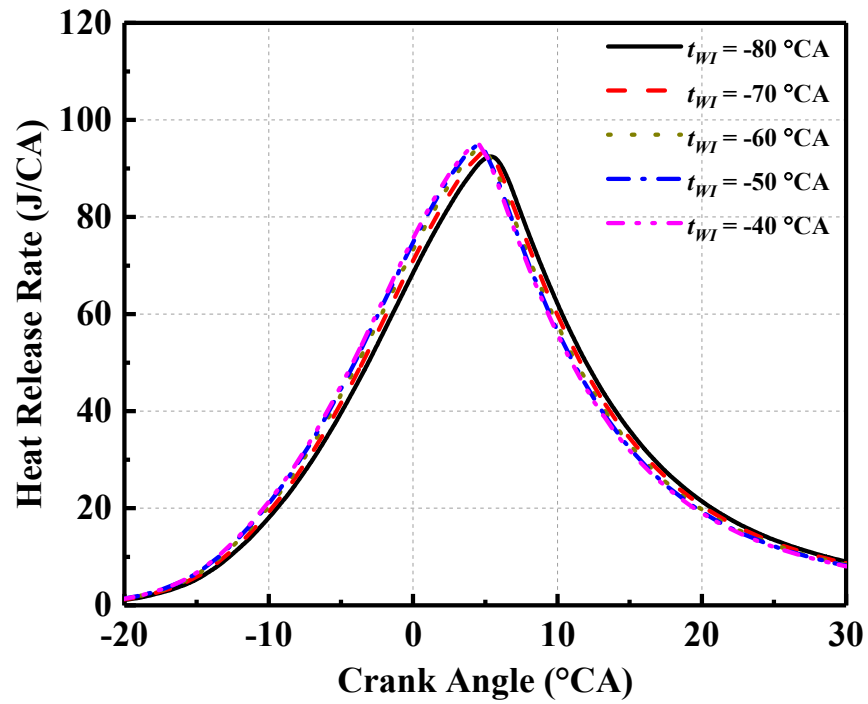
However, under the conditions of large  $R_{wf}$ , an apparent deterioration of BSFC<sub>E</sub> can be found with an inappropriate  $t_{WI}$ . For example, when  $R_{wf} = 0.6$ , BSFC<sub>E</sub> could be increased to 320.992 g/kWh and 319.726 g/kWh for  $t_{WI} = -100^\circ\text{CA}$  and  $t_{WI} = -30^\circ\text{CA}$ , respectively. The gap in BSFC<sub>E</sub> between  $t_{WI} = -100^\circ\text{CA}$  and  $t_{WI} = -60^\circ\text{CA}$  can be up to around 6.3 g/kWh. This demonstrates that BSFC<sub>E</sub> is particularly sensitive to  $t_{WI}$  under high  $R_{wf}$  conditions, which should be of concern for a GDI engine operating under OFC mode.

To explore the reasons for the variation in BSFC<sub>E</sub> affected by  $t_{WI}$ , the change in HRR is studied under  $R_{wf} = 0.1$  and  $R_{wf} = 0.6$ , as shown in Figure 11. The overall trend is that HRR could be influenced by continuously changing  $t_{WI}$ , and the degree of influence can be enhanced with a higher  $R_{wf}$ . When  $R_{wf} = 0.1$ , the HRR peak only increases by 2 J/ $^\circ\text{CA}$ , while the phase just advances from 5.6 $^\circ\text{CA}$  to 4.4 $^\circ\text{CA}$ . Under  $R_{wf} = 0.6$ , as  $t_{WI}$  postpones from  $-80^\circ\text{CA}$  to  $-40^\circ\text{CA}$ , the phase of the HRR peak monotonically advances from 7.2 $^\circ\text{CA}$  to 4.2 $^\circ\text{CA}$ . Meanwhile, the peak of HRR is increased by approximately 7 J/ $^\circ\text{CA}$ . This suggests that the excessively advanced  $t_{WI}$  could result in sufficient water vaporisation, which postpones the heat release and combustion phase. Therefore, it is essential to look for an optimal  $t_{WI}$  to increase thermal efficiency, especially under the conditions of large  $R_{wf}$ .

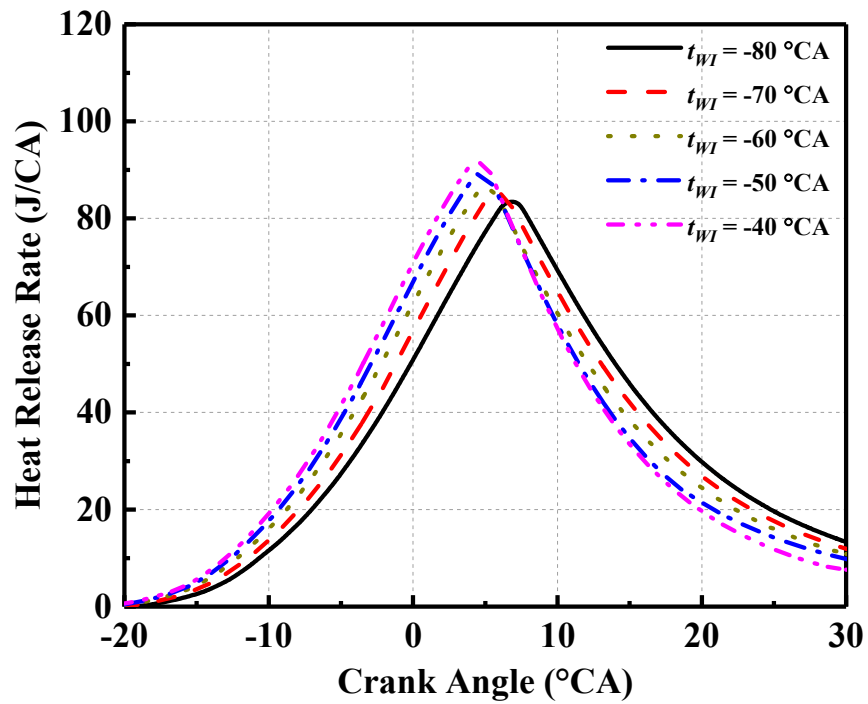
As shown in Figure 12, the in-cylinder temperature can be influenced by the variation of  $t_{WI}$ . Under  $R_{wf} = 0.1$ , as  $t_{WI}$  postpones from  $-80^\circ\text{CA}$  to  $-40^\circ\text{CA}$ , the maximum in-cylinder temperature increases from 2175 K to 2191 K, with an improvement of around 16 K. Furthermore, the degree of influence on in-cylinder temperature is increased significantly with a higher  $R_{wf}$ . When the  $R_{wf}$  reaches 0.6, the relevant improvement of maximum in-cylinder temperature can be up to 64 K. This can be attributed to the fact that stronger cooling effects can be achieved with a relatively high amount of injected water under  $t_{WI} = -80^\circ\text{CA}$ .

Figure 13 shows the variation in  $P_M$  and  $\varphi_{CA50}$  with different  $t_{WI}$ . The  $P_M$  shows a monotonic increasing trend as  $t_{WI}$  postpones from  $-100^\circ\text{CA}$  to  $-30^\circ\text{CA}$ . Under  $R_{wf} = 0.1$ ,  $P_M$  has an improvement of around 2.3 bar. Meanwhile, the change in magnitude is about 11 bar under  $R_{wf} = 0.6$ . On the contrary,  $\varphi_{CA50}$  shows a highly advanced trend by postponing  $t_{WI}$ . When  $t_{WI}$  postpones from  $-100^\circ\text{CA}$  to  $-30^\circ\text{CA}$ , an advance of about 1.5 $^\circ\text{CA}$  can be seen in  $\varphi_{CA50}$  under  $R_{wf} = 0.1$ , whilst an advance of about 7 $^\circ\text{CA}$  occurs under  $R_{wf} = 0.6$ . By postponing  $t_{WI}$ , the variation characteristics of  $P_M$  and  $\varphi_{CA50}$  are mainly because the short water vaporisation period weakens the inhibition impact on combustion.

From Figure 13, it is notable that when  $t_{WI}$  is  $-40^\circ\text{CA}$  and  $-30^\circ\text{CA}$ , the distinction of these combustion characteristics between  $R_{wf} = 0.1$  and  $R_{wf} = 0.6$  become quite slight. That is because under the conditions of a late  $t_{WI}$ , the effects of  $t_{WI}$  on  $P_M$  and  $\varphi_{CA50}$  become relatively small due to the shorter water vaporisation period before combustion.



(a)



(b)

Figure 11. Effects of  $t_{WI}$  on HRR. (a)  $R_{wf} = 0.1$ . (b)  $R_{wf} = 0.6$ .

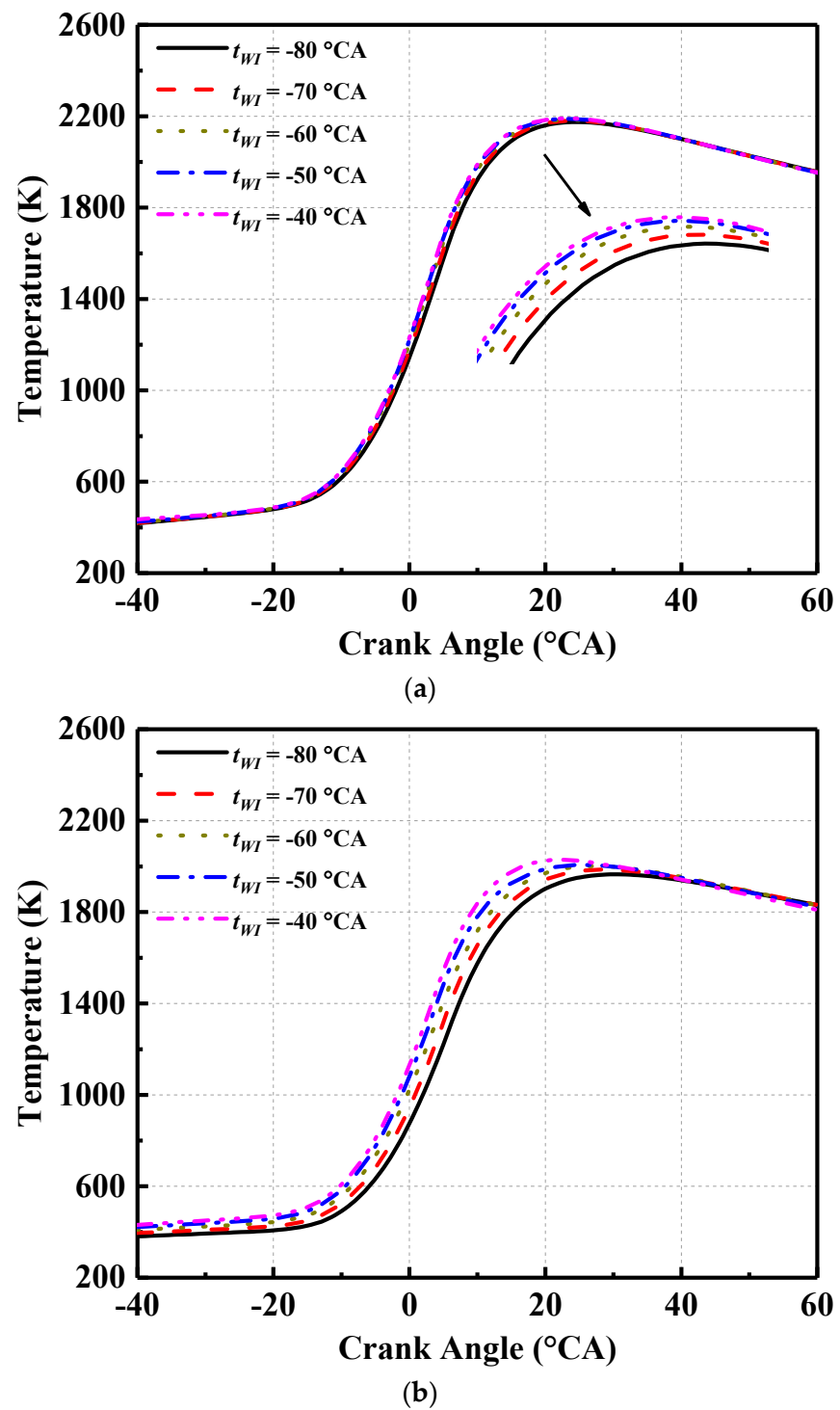


Figure 12. Effects of  $t_{WI}$  on in-cylinder temperature. (a)  $R_{wf} = 0.1$ . (b)  $R_{wf} = 0.6$ .

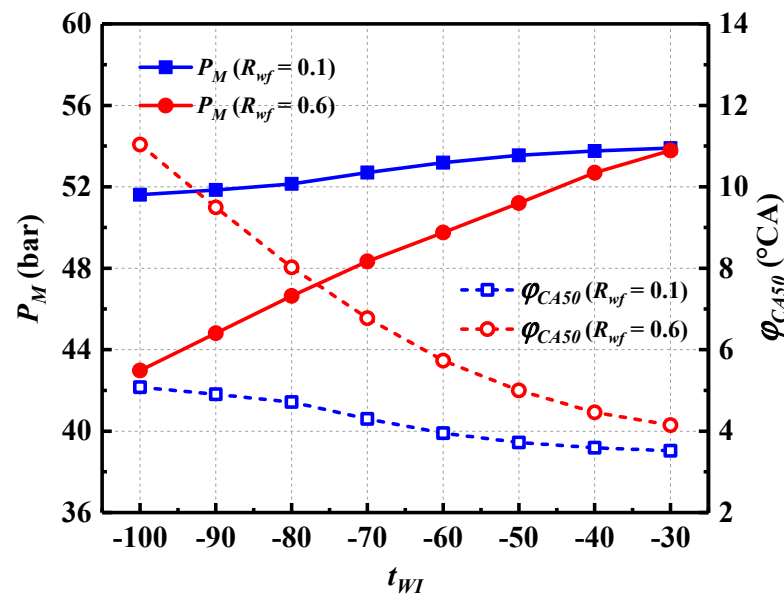


Figure 13. Effects of  $t_{WI}$  on  $P_{max}$  and  $\varphi_{CA50}$ .

#### 4. Conclusions

The OFC technique has shown great potential in achieving zero CO<sub>2</sub> emissions from conventional GDI engines. To further improve the fuel economy of engines under OFC mode, this study numerically investigates the effects of WI strategies on OFC characteristics in a GDI engine fuelled with E10. The main conclusions can be listed as follows.

1. Under OFC mode without WI strategy, the optimum BSFC<sub>E</sub> is 311.35 g/kWh by advancing spark timing to  $-72^\circ$ CA.
2. BSFC<sub>E</sub> shows a monotonically decreasing trend by increasing  $R_{wf}$  from 0 to 0.2, due to the increasing oxygen concentration caused by the decomposition of water.
3. With the increase in  $R_{wf}$  from 0.2 to 0.9, strong cooling effects significantly decrease the in-cylinder temperature and postpone the heat release. Hence, a deterioration is caused owing to a larger  $R_{wf}$ .
4. In general, BSFC<sub>E</sub> is largely unaffected by  $t_{WI}$  when  $R_{wf}$  is 0.1 and 0.2. BSFC<sub>E</sub> can be optimised to 310.735 g/kWh under the condition of  $t_{WI} = -100^\circ$ CA and  $R_{wf} = 0.1$ .
5. Under the conditions of a late  $t_{WI}$ , the effects of  $t_{WI}$  on  $P_M$  and  $\varphi_{CA50}$  become relatively small due to the shorter water vaporisation period before combustion.
6. An appropriate  $t_{WI}$  is very important to improve the OFC performance under large  $R_{wf}$  conditions. When  $R_{wf}$  reaches 0.6, the gap in BSFC<sub>E</sub> between  $t_{WI} = -100^\circ$ CA and  $t_{WI} = -60^\circ$ CA can be up to around 6.3 g/kWh.

According to the findings of this study, water injection mass and timing have been proven to effectively impact the combustion characteristics and fuel economy of GDI engines fuelled with E10 under OFC mode. Several proposals can be forwarded as follows regarding the prospects for future studies in the specific knowledge area.

First, some other key parameters of WI strategy can be explored and studied for GDI engines under OFC mode. For instance, increasing the WI pressure could be a potential solution to optimise the combustion process and fuel efficiency by shorting the WI duration under the conditions of fixed WI mass. The change in WI temperature is also a factor that affects combustion quality, which can be a research direction.

Second, it is necessary to investigate OFC GDI engines fuelled with a high ethanol ratio in the gasoline–alcohol blends. Changing the ethanol ratio in blends impacts the fuel's physicochemical properties, thereby resulting in a significant discrepancy in engine performance.

Third, it is also valuable to study the most suitable EGR rate to impact fuel performance for OFC engines fuelled with gasoline–alcohol blends. In the meantime, oxygen

consumption rates should be noted, which will be a cost factor during the operation of OFC engines.

**Author Contributions:** H.C.: methodology, visualisation, writing—original draft. C.W.: formal analysis, investigation, visualisation, writing—original draft. X.L.: conceptualisation, methodology, investigation, visualisation, writing—original draft, writing—reviewing and editing. Y.L.: formal analysis. M.Z.: writing—reviewing and editing. Z.P.: conceptualisation. Y.P.: methodology. Z.M.: conceptualisation. X.Z.: visualisation. P.N.: formal analysis. R.W.: conceptualisation. R.M.: methodology. All authors have read and agreed to the published version of the manuscript.

**Funding:** This work was supported by the European Regional Development Fund (ERDF) via Interreg North-West Europe (Project No. NWE553).

**Institutional Review Board Statement:** Not applicable.

**Informed Consent Statement:** Not applicable.

**Data Availability Statement:** Not applicable.

**Conflicts of Interest:** The authors declare no conflict of interest.

### Abbreviations

BEVs	Battery Electric Vehicles
BMEP	Brake Mean Effective Pressure
BSFC	Brake Specific Fuel Consumption
BSFC <sub>E</sub>	Equivalent Brake-Specific Fuel Consumption
CA	Crank Angle
CAC	Conventional Air Combustion
CCS	Carbon Capture and Storage
CO <sub>2</sub>	Carbon Dioxide
E10	10% ethanol and 90% gasoline in mass
ECU	Electronic Control Unit
EGR	Exhaust Gas Recirculation
ERDF	European Regional Development Fund
GDI	Gasoline Direct Injection
HCCI	Homogeneous Charge Compression Ignition
HRR	Heat Release Rate
ICE	Internal Combustion Engine
ICRC	Internal Combustion Rankine Cycle
KLSA	Knock Limited Spark Advance
MBT	Maximum Brake Torque
OFC	Oxy-Fuel Combustion
PFI	Port Fuel Injection
SI	Spark Ignition
WI	Water Injection
$R_{wf}$	Water–Fuel mass ratio
$t_{WI}$	Water Injection Timing

### References

1. Rousi, E.; Kornhuber, K.; Beobide-Arsuaga, G.; Luo, F.; Coumou, D. Accelerated western European heatwave trends linked to more-persistent double jets over Eurasia. *Nat. Commun.* **2022**, *13*, 3851. [[CrossRef](#)]
2. Zhao, X.; Doering, O.C.; Tyner, W.E. The economic competitiveness and emissions of battery electric vehicles in China. *Appl. Energy* **2015**, *156*, 666–675. [[CrossRef](#)]
3. Zareei, J.; Rohani, A. Optimization and study of performance parameters in an engine fueled with hydrogen. *Int. J. Hydrogen Energy* **2020**, *45*, 322–336. [[CrossRef](#)]
4. Lhuillier, C.; Brequigny, P.; Contino, F.; Mounaïm-Rousselle, C. Experimental study on ammonia/hydrogen/air combustion in spark ignition engine conditions. *Fuel* **2020**, *269*, 117448. [[CrossRef](#)]
5. Li, Z.; Wang, W.; Ye, M.; Liang, X. The impact of hydrogen refueling station subsidy strategy on China's hydrogen fuel cell vehicle market diffusion. *Int. J. Hydrogen Energy* **2021**, *46*, 18453–18465. [[CrossRef](#)]

6. Nozaki, T.; Takano, S.I.; Kiga, T.; Omata, K.; Kimura, N. Analysis of the flame formed during oxidation of pulverized coal by an O<sub>2</sub>/CO<sub>2</sub> mixture. *Energy* **1997**, *22*, 199–205. [[CrossRef](#)]
7. Mondal, M.K.; Balsora, H.K.; Varshney, P. Progress and trends in CO<sub>2</sub> capture/separation technologies: A review. *Energy* **2012**, *46*, 431–441. [[CrossRef](#)]
8. Stanger, R.; Wall, T.; Spörl, R.; Paneru, M.; Grathwohl, S.; Weidmann, M.; Scheffknecht, G.; McDonald, D.; Myöhänen, K.; Ritvanen, J.; et al. Oxyfuel combustion for CO<sub>2</sub> capture in power plants. *Int. J. Greenh. Gas Control* **2015**, *40*, 55–125. [[CrossRef](#)]
9. Li, X.; Peng, Z.; Pei, Y.; Ajmal, T.; Rana, K.J.; Aitouche, A.; Mobasheri, R. Oxy-fuel combustion for carbon capture and storage in internal combustion engines—A review. *Int. J. Energy Res.* **2022**, *46*, 505–522. [[CrossRef](#)]
10. Wall, T.; Liu, Y.; Spero, C.; Elliott, L.; Khare, S.; Rathnam, R.; Zeenathal, F.; Moghtaderi, B.; Buhre, B.; Sheng, C.; et al. An overview on oxyfuel coal combustion—State of the art research and technology development. *Chem. Eng. Res. Des.* **2009**, *87*, 1003–1016. [[CrossRef](#)]
11. Chen, L.; Yong, S.Z.; Ghoniem, A.F. Oxy-fuel combustion of pulverized coal: Characterization, fundamentals, stabilization and CFD modeling. *Prog. Energy Combust. Sci.* **2012**, *38*, 156–214. [[CrossRef](#)]
12. Ditaranto, M.; Hals, J. Combustion instabilities in sudden expansion oxy–fuel flames. *Combust. Flame* **2006**, *146*, 493–512. [[CrossRef](#)]
13. Li, X.; Pei, Y.; Ajmal, T.; Rana, K.J.; Aitouche, A.; Mobasheri, R.; Peng, Z. Numerical investigation on implementing Oxy-Fuel Combustion (OFC) in an ethanol-gasoline Dual-Fuel Spark Ignition (DFSI) engine. *Fuel* **2021**, *302*, 121162. [[CrossRef](#)]
14. Yu, X.; Wu, Z.; Fu, L.; Deng, J.; Hu, Z.; Li, L. Study of Combustion Characteristics of a Quasi Internal Combustion Rankine Cycle Engine. In *SAE Technical Paper*; SAE International: Warrendale, PA, USA, 2013.
15. Bilger, R.W.; Wu, Z. Carbon capture for automobiles using internal combustion Rankine cycle engines. *J. Eng. Gas Turbines Power* **2009**, *131*, 034502. [[CrossRef](#)]
16. Fu, L.-Z.; Wu, Z.; Li, L.; Yu, X. Effect of Water Injection Temperature on Characteristics of Combustion and Emissions for Internal Combustion Rankine Cycle Engine. In *SAE Technical Paper*; SAE International: Warrendale, PA, USA, 2014.
17. Wu, Z.J.; Yu, X.; Fu, L.Z.; Deng, J.; Hu, Z.J.; Li, L.G. A high efficiency oxyfuel internal combustion engine cycle with water direct injection for waste heat recovery. *Energy* **2014**, *70*, 110–120. [[CrossRef](#)]
18. Kang, Z.; Wu, Z.; Zhang, Z.; Deng, J.; Hu, Z.; Li, L. Study of the combustion characteristics of a HCCI engine coupled with oxy-fuel combustion mode. *SAE Int. J. Engines* **2017**, *10*, 908–916. [[CrossRef](#)]
19. Kang, Z.; Chen, S.; Wu, Z.; Deng, J.; Hu, Z.; Li, L. Simulation Study of Water Injection Strategy in Improving Cycle Efficiency Based on a Novel Compression Ignition Oxy-Fuel Combustion Engine. *SAE Int. J. Engines* **2018**, *11*, 935–945. [[CrossRef](#)]
20. Li, X.; Pei, Y.; Li, D.; Ajmal, T.; Rana, K.-J.; Aitouche, A.; Mobasheri, R.; Peng, Z. Effects of Water Injection Strategies on Oxy-Fuel Combustion Characteristics of a Dual-Injection Spark Ignition Engine. *Energies* **2021**, *14*, 5287. [[CrossRef](#)]
21. Liu, K.; Li, Y.; Yang, J.; Deng, B.; Feng, R.; Huang, Y. Comprehensive study of key operating parameters on combustion characteristics of butanol-gasoline blends in a high speed SI engine. *Appl. Energy* **2018**, *212*, 13–32. [[CrossRef](#)]
22. Tornatore, C.; Bozza, F.; De Bellis, V.; Teodosio, L.; Valentino, G.; Marchitto, L. Experimental and Numerical Study on the Influence of Cooled EGR on Knock Tendency, Performance and Emissions of a Downsized Spark-Ignition Engine. *Energy* **2019**, *172*, 968–976. [[CrossRef](#)]
23. Song, R.; Liu, J.; Wang, L.; Liu, S. Performance and emissions of a diesel engine fuelled with methanol. *Energy Fuels* **2008**, *22*, 3883–3888. [[CrossRef](#)]
24. How, H.G.; Masjuki, H.H.; Kalam, M.A.; Teoh, Y.H. An investigation of the engine performance, emissions and combustion characteristics of coconut biodiesel in a high-pressure common-rail diesel engine. *Energy* **2014**, *69*, 749–759. [[CrossRef](#)]
25. Liu, J.; Duan, X.; Yuan, Z.; Liu, Q.; Tang, Q. Experimental study on the performance, combustion and emission characteristics of a high compression ratio heavy-duty spark-ignition engine fuelled with liquefied methane gas and hydrogen blend. *Appl. Therm. Eng.* **2017**, *124*, 585–594. [[CrossRef](#)]
26. Kang, R.; Zhou, L.; Hua, J.; Feng, D.; Wei, H.; Chen, R. Experimental investigation on combustion characteristics in dual-fuel dual-injection engine. *Energy Convers. Manag.* **2019**, *181*, 15–25. [[CrossRef](#)]
27. Biswas, S.; Kakati, D.; Chakraborti, P.; Banerjee, R. Assessing the potential of ethanol in the transition of biodiesel combustion to rcci regimes under varying injection phasing strategies: A performance-emission-stability and tribological perspective. *Fuel* **2021**, *304*, 121346. [[CrossRef](#)]
28. Woschni, G. A Universally Applicable Equation for the Instantaneous Heat Transfer Coefficient in the Internal Combustion Engine. In *SAE Technical Paper*; SAE International: Warrendale, PA, USA, 1967.

**Disclaimer/Publisher’s Note:** The statements, opinions and data contained in all publications are solely those of the individual author(s) and contributor(s) and not of MDPI and/or the editor(s). MDPI and/or the editor(s) disclaim responsibility for any injury to people or property resulting from any ideas, methods, instructions or products referred to in the content.